Matter and Radiation at Extremes | RESEARCH ARTICLE | scitation.org/journal/mre

Cerium-promoted conversion of dinitrogen into high-energy-density material CeN_6 under moderate pressure

Cite as: Matter Radiat. Extremes 8, 038401 (2023); doi: 10.1063/5.0136443
Submitted: 26 November 2022 • Accepted: 16 March 2023 •
Published Online: 20 April 2023

View Online Export Citation CrossMark

Yuanyuan Wang,[1] Zhihui Li,[1] Shifeng Niu,[2] Wencai Yi,[3,a)] Shuang Liu,[1,a)] Zhen Yao,[1,a)] and Bingbing Liu[1,a)]

AFFILIATIONS

[1] State Key Laboratory of Superhard Materials, College of Physics, Jilin University, Changchun 130012, People's Republic of China
[2] Henan Key Laboratory of Photoelectric Energy Storage Materials and Applications, School of Physics and Engineering, Henan University of Science and Technology, Luoyang 471023, People's Republic of China
[3] Laboratory of High Pressure Physics and Material Science (HPPMS), School of Physics and Physical Engineering, Qufu Normal University, Qufu, Shandong 273165, People's Republic of China

[a)] **Authors to whom correspondence should be addressed:** yiwc@qfnu.edu.cn, liu_shuang@jlu.edu.cn, yaozhen@jlu.edu.cn, and liubb@jlu.edu.cn

ABSTRACT

Synthesis pressure and structural stability are two crucial factors for highly energetic materials, and recent investigations have indicated that cerium is an efficient catalyst for N_2 reduction reactions. Here, we systematically explore Ce–N compounds through first-principles calculations, demonstrating that the cerium atom can weaken the strength of the N≡N bond and that a rich variety of cerium polynitrides can be formed under moderate pressure. Significantly, $P\bar{1}$-CeN_6 possesses the lowest synthesis pressure of 32 GPa among layered metal polynitrides owing to the strong ligand effect of cerium. The layered structure of $P\bar{1}$-CeN_6 proposed here consists of novel N_{14} ring. To clarify the formation mechanism of $P\bar{1}$-CeN_6, the reaction path Ce + $3N_2$ → *trans*-CeN_6 → $P\bar{1}$-CeN_6 is proposed. In addition, $P\bar{1}$-CeN_6 possesses high hardness (20.73 GPa) and can be quenched to ambient conditions. Charge transfer between cerium atoms and N_{14} rings plays a crucial role in structural stability. Furthermore, the volumetric energy density (11.20 kJ/cm^3) of $P\bar{1}$-CeN_6 is much larger than that of TNT (7.05 kJ/cm^3), and its detonation pressure (128.95 GPa) and detonation velocity (13.60 km/s) are respectively about seven times and twice those of TNT, and it is therefore a promising high-energy-density material.

I. INTRODUCTION

Polymeric nitrogen materials are environmentally friendly high-energy-density materials (HEDMs). Their high energy density comes from the huge energy difference between the N≡N triple bond (954 kJ/mol) on the one hand and the N=N double and N–N single bonds (418 and 160 kJ/mol, respectively) on the other. To date, a wide variety of novel polynitrogen structures have been reported in theoretical studies, such as the three-dimensional (3D) network structures (*cg*-N, *Pnnm*, *Cccm*, and CW),[1–3] two-dimensional (2D) layer structures (A7, ZS, LB, LP, HLP, PP, and BP phases),[4–9] one-dimensional (1D) chain structures (ch-N and *Cmcm*),[10] and a zero-dimensional (0D) cage structure (N_{10}).[11] High temperature and high pressure are two important factors in obtaining polynitrogen materials. However, the ultrahigh pressure (>100 GPa) and temperature (>2000 K) in experiment required for the synthesis of *cg*-N, LP-N, HLP-N, and BP-N limit their development.[12–15] An additional challenge is posed in quenching the high-pressure phases to ambient conditions, owing to their intrinsic metastable properties. Therefore, reducing the synthesis pressure and enhancing the structural stability of polynitrogen materials are crucial for their practical application. Nitrogen-rich compounds have been demonstrated to be promising candidates to achieve these goals.

In experiments, LiN_5, K_2N_6, MgN_4, Mg_2N_4, CsN_5, α-ZnN_4, β-ZnN_4, and *tr*-BeN_4 have been synthesized at pressures of 45, 45, 50, 50, 60, 63.5, 81.7, and 85 GPa, respectively.[16–21] Moreover, LiN_5, Mg_2N_4, and *tr*-BeN_4 can be quenched down to ambient conditions. Clearly, compared with polynitrogen structures, nitrogen-rich compounds have milder synthesis conditions and higher stability. Theoretically, they exhibit a wide variety of nitrogen configurations, ranging from N_2 dumbbells,[22,23] azide roots,[24–26] N rings (N_4,[27,28] N_5,[29–34] and N_6[35–37]), 1D N chains,[38–43] 2D N layers,[44–49] to 3D network structures.[50,51] Recently, the lanthanide polynitrides $P\bar{1}$-GdN_6 and $P\bar{1}$-ErN_6 have been proposed as HEDMs with excellent explosive performance.[52,53] As a typical lanthanide element, cerium (Ce) is the most abundant rare earth element in the Earth's crust and much cheaper than most rare earth metals, such as Gd and Er. Additionally, Ce atoms possess flexible electronic properties that allow them to reach high coordination numbers in their compounds. Thus, they exhibit excellent performance in the selective catalytic reduction of N_2 to NH_3.[54–56] In light of these characteristics, we suggest that Ce may be an ideal candidate for inducing polynitrogen structures. However, up until now, only CeN has been reported in high-pressure studies,[57–59] which has motivated us to perform a systematic high-pressure study on nitrogen-rich Ce–N compounds.

In this work, we systematically study Ce–N high-pressure compounds at pressures up to 100 GPa through first-principles swarm-intelligence structural searches. Seven stoichiometric ratios of CeN_n (n = 0.5, 1, 2, 3, 4, 5, and 6) compounds are explored. Six new high-pressure phases are proposed, and their stability is verified using phonon dispersion curves, elastic constants, and molecular dynamic simulations. Interestingly, $P\bar{1}$-CeN_6 not only possesses the lowest synthesis pressure of 32 GPa among layered metal polynitrides, but also can be quenched to ambient conditions. The stability mechanism of $P\bar{1}$-CeN_6 is clarified by electronic structure and bonding analyses, and its mechanical properties are analyzed. Its infrared spectra (IR) and Raman spectra are calculated for experimental reference. Significantly, $P\bar{1}$-CeN_6 shows excellent volumetric energy density (up to 11.20 kJ/cm^3), detonation pressure (128.95 GPa), and detonation velocity (13.60 km/s), opening up exciting avenues for the exploration of high-nitrogen-concentration lanthanide polynitrides via the metal ligand effect.

II. CALCULATION DETAILS

The structure searches were performed using the particle swarm optimization structure prediction method in the CALYPSO code.[60] Seven stoichiometric ratios of CeN_n (n = 0.5, 1, 2, 3, 4, 5, and 6) compounds were considered in the structural prediction at 0, 20, 50, and 100 GPa. The simulation cells contained 1, 2, and 4 formula units (f.u.), in which a total of 75 600 structures were produced and were ranked according to the calculated enthalpy. The previously reported $Fm\bar{3}m$-CeN and $P4/nmm$-CeN were successfully reproduced in our search,[58] validating the effectiveness of the method. The structural relaxations and property calculation were performed using the Vienna *Ab initio* Simulation Package (VASP).[61] The generalized gradient approximation (GGA) was used with the Perdew–Burke–Ernzerhof (PBE) exchange correlation functional.[62] The GGA + U method (U = 6 eV) was used to correct the strong on-site Coulomb repulsion of Ce_4f states.[63–66] The valence electrons of Ce and N atoms in the projector augmented wave (PAW) pseudopotentials were $4f^1 5d^1 6s^2$ *and* $2s^2 2p^3$, respectively.[67] The Monkhorst–Pack k mesh spacing density and plane wave energy cutoff were set to $2\pi \times 0.03$ Å^{-1} and 520 eV, respectively. The accurate band structure was obtained using a hybrid functional (HSE06).[68] The enthalpies of formation ΔH_f of the CeN_n compounds were calculated using the equation

$$\Delta H_f(CeN_n) = \frac{H(CeN_n) - H(Ce) - nH(N)}{1+n}.$$

The phonon dispersion curves were obtained using the PHONOPY code with density-functional perturbation theory.[69] The energy density was calculated by considering the following dissociation path under ambient pressure: $CeN_n \rightarrow CeN + \frac{1}{2}(n-1)N_2$. The detonation velocity and detonation pressure were calculated from the Kamlet–Jacobs semiempirical equations[70] $V_d = 1.01(NM^{0.5}E_d^{0.5})^{0.5}(1+1.30\rho)$ and $P_d = 15.58\rho^2 NM^{0.5}E_d^{0.5}$. The *ab initio* molecular dynamics (AIMD) simulations were performed in the isobaric–isothermic (*NPT*) ensemble with a total simulation time of 10 ps.[71] The crystal orbital Hamilton population (COHP) was calculated using the LOBSTER package.[72] For Raman and IR spectra, norm-conserving pseudopotentials were adopted, and these were calculated using the CASTEP module of the Material Studio package. Convergence criteria consisted of an energy change of $<2 \times 10^{-5}$ eV/atom and a maximum force of <0.05 eV/Å.[73]

III. RESULTS AND DISCUSSION

A. Phase diagram and structural stability

The convex hull of CeN_n compounds is calculated for screening the thermodynamically stable phases of optimal structures in the prediction, and the results show that Ce can promote the formation of various polynitrides under high pressure. The stable phases of solid cerium ($Fm\bar{3}m$ and $Cmcm$ phases) and solid nitrogen ($Pa\bar{3}$, $P4_2/mnm$, $P4_12_12$, and *cg*-N phases) are used as the references to calculate the formation enthalpy ΔH_f, and this is plotted in Fig. 1(a), where the solid and blank squares correspond to the thermodynamically stable and unstable/metastable phases, respectively. The phase diagrams of thermodynamically stable high-pressure structures are obtained from the enthalpy difference analysis and are shown in Fig. 1(b) and Fig. S1 in the supplementary material. It can be seen that $Fm\bar{3}m$-CeN is stable from 0 to 69 GPa and then transforms to $P4/nmm$-CeN. This phase transition pressure is consistent with a previous experimental result (65 GPa).[58] $I4/mmm$-CeN_2 remains stable at 8–100 GPa. $C2/m$-CeN_3 is stable above 6 GPa, and then changes to $P\bar{1}$-CeN_3 at 82 GPa. As the nitrogen concentration increases, $P\bar{1}$-CeN_4 remains stable in the pressure range of 32–100 GPa. At 20 and 50 GPa, we predicted $C2/c$-CeN_6 and $P\bar{1}$-CeN_6 phases, which are energetically favorable at 9–32 GPa and 32–100 GPa, respectively. Interestingly, as far as we know, the synthesis pressure (32 GPa) of $P\bar{1}$-CeN_6 is the lowest among the layered metal polynitrides.

The crystal structures of CeN_n compounds reveal that Ce has strong coordination ability under high pressure [Figs. 2 and S2 (supplementary material)], with each Ce atom coordinating with 10, 8, 10, 10, 10, and 12 N atoms in $I4/mmm$-CeN_2, $C2/m$-CeN_3, $P\bar{1}$-CeN_3, $P\bar{1}$-CeN_4, $C2/c$-CeN_6, and $P\bar{1}$-CeN_6, respectively [Fig. S3 (supplementary material)]. The N-structure units in $I4/mmm$-CeN_2 and $C2/c$-CeN_6 are N_2 dumbbells, and those in $C2/m$-CeN_3 and $P\bar{1}$-CeN_3 are N_2 dumbbells and N_4 molecular chains. The

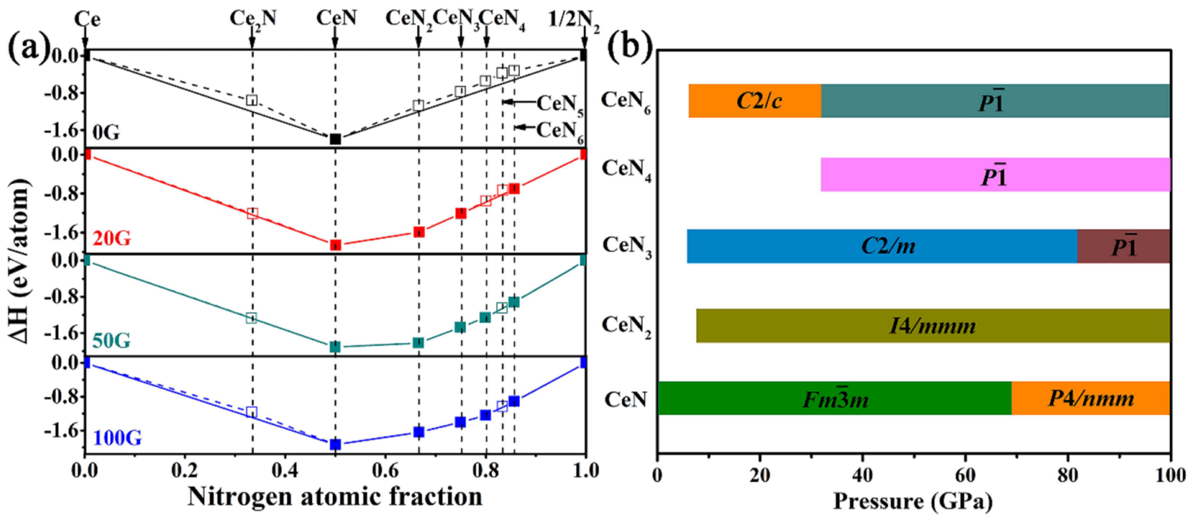

FIG. 1. (a) Formation enthalpies ΔH of various CeN_n (n = 0.5, 1, 2, 3, 4, 5, and 6) compounds under high pressure. The stable phases are connected by solid lines and unstable/metastable phases by dashed lines. (b) Pressure–composition phase diagram of the predicted Ce–N phases.

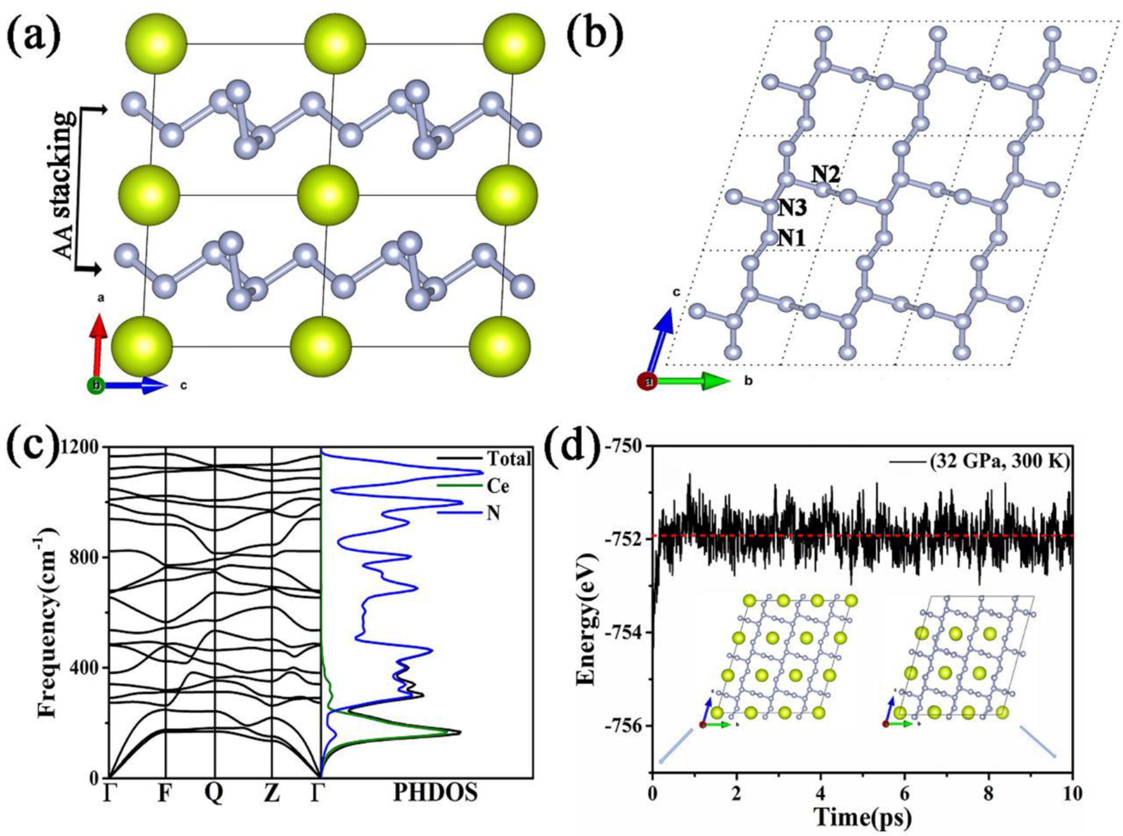

FIG. 2. (a) Crystal structure of $P\bar{1}$-CeN_6 at 32 GPa. (b) Nitrogen structural skeleton of $P\bar{1}$-CeN_6 at 32 GPa. The independent N atoms are marked as N1, N2, and N3 in the symmetric N_{14} rings. (c) Phonon dispersion curve and PHDOS of $P\bar{1}$-CeN_6 at 32 GPa. (d) Initial and terminal structures in AIMD simulations with total simulation time 10 ps and fluctuations of the total energy of $P\bar{1}$-CeN_6 at 32 GPa and 300 K.

polymeric structures of $P\bar{1}$-CeN_4 and $P\bar{1}$-CeN_6 are N_8 molecular chains and layered structures with an N_{14} ring, respectively [Fig. S4 (supplementary material)]. Calculations of phonon dispersion curves show that the six new CeN_n compounds described above are dynamically stable at predicted pressures owing to the absence of an imaginary frequency in the Brillouin zone [Fig. S5 (supplementary material)], and thus they are high-pressure stable phases. The structural parameters are listed in Table SI (supplementary material). Excluding $C2/c$-CeN_6, the average N–N bond length in CeN_n compounds is about 1.30–1.39 Å [Table SII (supplementary material)], which is much larger than that in nitrogen molecules (1.11 Å), suggesting that these represent a new type of nitrogen-rich materials in which the N–N bonds are single or intermediate between single and double in nature. We deduce that they may have high energy capacity properties.

Among these CeN_n compounds, $P\bar{1}$-CeN_6 is particularly fascinating and worthy of further discussion because of its high nitrogen concentration, long N–N bonds, high coordination number, and low synthesis pressure. As shown in Fig. 2, the crystal structure of $P\bar{1}$-CeN_6 is layered, with an AαAα stacking form along the *a*-axis direction, where A and α represent the N plane and Ce plane, respectively. Interestingly, $P\bar{1}$-CeN_6 possesses unique N_{14} rings, the first to be reported up until now. At 32 GPa, the bond lengths of N1–N1, N1–N3, N3–N3, N3–N2, and N2–N2 are 1.40, 1.42, 1.47, 1.35, and 1.45 Å, respectively, indicating that the N3–N2 bond is intermediate in nature between a single bond (1.45 Å) and a double bond (1.25 Å), whereas all the other bonds are close to single bond in nature. The mechanical and dynamical stability of $P\bar{1}$-CeN_6 were verified at 32 GPa by calculating elastic constants and phonon dispersion curves [Fig. 2(c) and Table SIII (supplementary material)]. The phonon density of states (PHDOS) in Fig. 2(c) shows that the high-frequency vibrational modes come from N–N vibrations, while the low-frequency vibrational modes consist of Ce–N collective motions. Moreover, the thermal stability of $P\bar{1}$-CeN_6 was evaluated using AIMD simulations. As shown in Fig. 2(d), the total energy of $P\bar{1}$-CeN_6 fluctuates around the equilibrium position (−751.92 eV), and the structural skeleton remains intact at the end of the simulation, suggesting that $P\bar{1}$-CeN_6 is thermally stable under a pressure of 32 GPa and a temperature of 300 K.

B. Stability mechanism under high pressure

To pinpoint the stability mechanism of $P\bar{1}$-CeN_6, we carefully analyzed the electron localization function (ELF). As shown in Fig. 3(a), the N1 atoms in $P\bar{1}$-CeN_6 hybridize in sp^2 states with two σ bonds and a lone electron pair. Both the N2 and N3 atoms are sp^3 hybridized. The hybrid orbital of N2 atoms contains two σ bonds and two lone electron pairs, and that of the N3 atom contains three σ bonds and a lone electron pair. Additionally, the strong localization of electrons between N atoms indicates a strong N–N covalent bond interaction, and the lone-pair electrons of N atoms form strong coordination bonds with Ce atoms. Considering that the coordination number of Ce is up to 12 in $P\bar{1}$-CeN_6, we deduce that electron transfer between the Ce atoms and N-structures play a crucial role in stabilizing $P\bar{1}$-CeN_6 at the relatively low synthesis pressure of 32 GPa.

To confirm our idea, Bader charges were calculated and clearly show the charge transfer for each Ce atoms and N-structures in stable CeN_n (n = 1, 2, 3, 4, and 6) compounds at 32 GPa. The amount of charge transferred increases with nitrogen content from Fm-$3m$-CeN to $C2/m$-CeN_3 [Fig. 3(b)], and the formation energy decreases from −4.37 to −5.83 eV/f.u., because the Ce atoms need to contribute a greater amount of charge in the N-rich phases than in the N-poor ones to stabilize the structure. As the nitrogen concentration continues to increase, the amount of charge transferred no longer increases, because the Ce atom reaches its highest valence. In spite of this, the excess nitrogen atoms can share electrons with others and form coordination bonds with Ce atoms, and hence the formation energy just increases from −5.83 eV/f.u. ($C2/m$-CeN_3) to −5.67 eV/f.u. ($P\bar{1}$-CeN_6). Consequently, the donor electrons and the strong ligand effect of Ce atoms are two important factors stabilizing high-nitrogen compounds.

To determine the unique ligand effect of Ce in $P\bar{1}$-CeN_6, we performed a comparative analysis by simulating the high-pressure polymerization behavior of N_2 molecules under two reaction environments. The projection of the COHP (pCOHP), the integral of the COHP (ICOHP), and the projected density of states (PDOS) were calculated to analyze the bonding features and bonding strength. According to the lattice parameters and stoichiometric ratio of $P\bar{1}$-CeN_6, we constructed a $P\bar{1}$-N_2 molecular crystal with six N atoms per cell, and made it more reasonable and stable by geometrical optimization at 32 GPa. The distance between the N_2 molecules decreases dramatically to about 2.37–2.45 Å [Fig. 4(a)], but it is still larger than length of an N–N single bond (1.45 Å), suggesting that there is no bonding reaction between N_2 molecules. The large −ICOHP (26.4) of the N–N bond and the strong hybridization interaction between N_2s and N_2p orbitals indicate strong

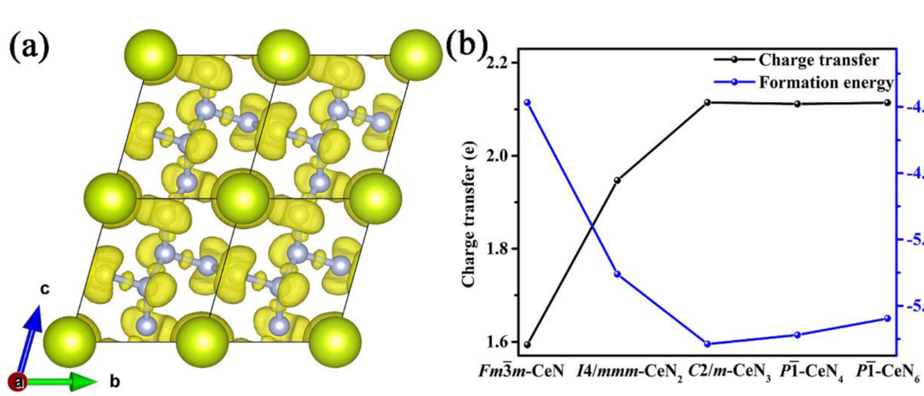

FIG. 3. (a) ELF of $P\bar{1}$-CeN_6 (isovalue = 0.8). (b) The charge transfer and formation energy of CeN_n (n = 1, 2, 3, 4 and 6) compounds at 32 GPa.

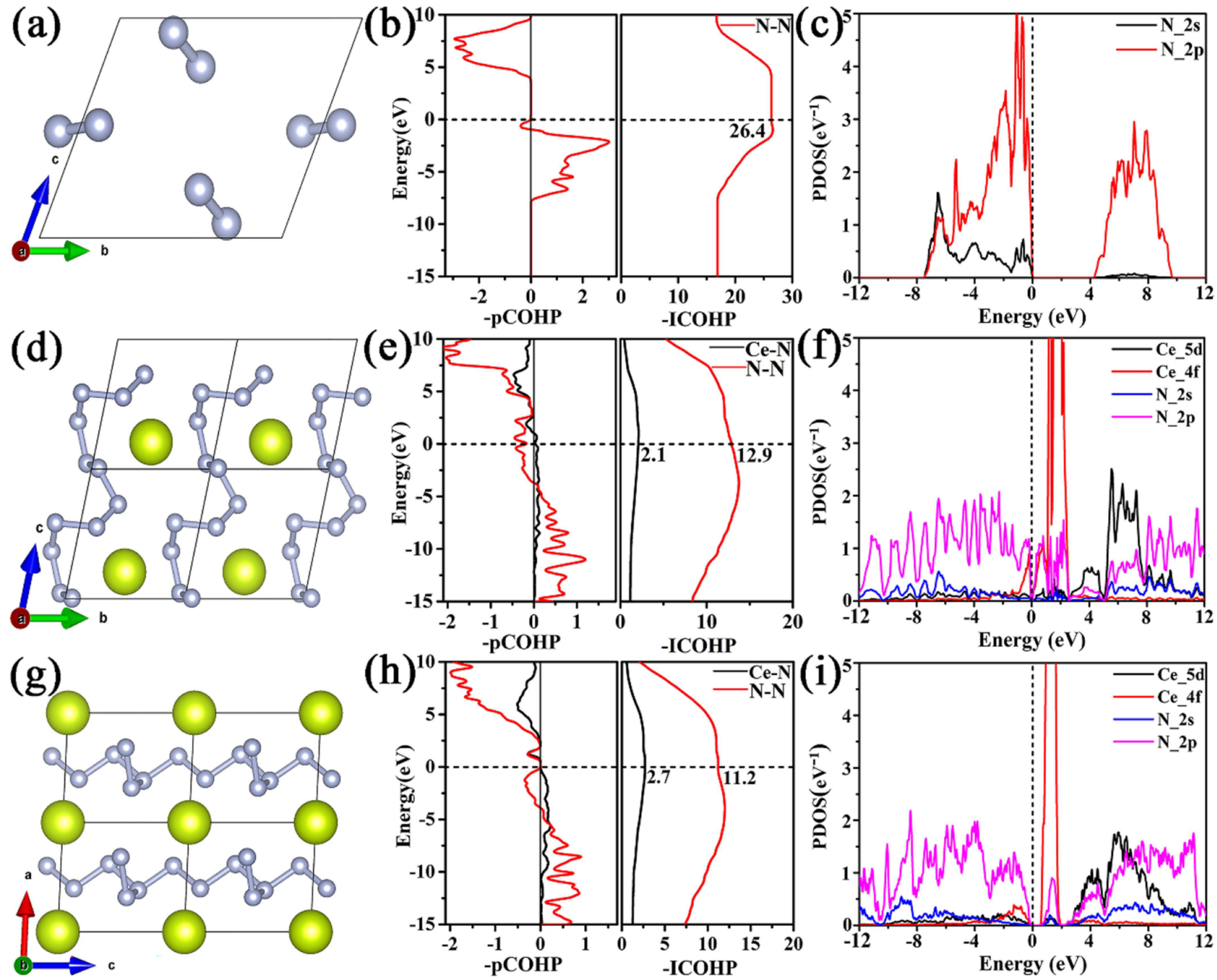

FIG. 4. (a) Crystal structure, (b) −pCOHP and −ICOHP, and (c) PDOS of N_2 molecular crystal. (d) Crystal structure, (e) −pCOHP and −ICOHP, and (f) PDOS of *trans*-CeN_6. (g) Crystal structure, (h) −pCOHP and −ICOHP, and (i) PDOS of $P\bar{1}$-CeN_6 at 32 GPa.

covalent interaction in the N–N bond [Figs. 4(b) and 4(c)]. All the above points support the fact that the N≡N triple bonds in N_2 molecules are hard to break down at 32 GPa.

However, when we insert a Ce atom into the body-centered position (0.5, 0.5, 0.5) of $P\bar{1}$-N_2, the transitional CeN_6 (*trans*-CeN_6) with *cis*-form N chains is formed after optimization at the same pressure [Fig. 4(d)]. The hybridization interaction between N_2*s* and N_2*p* orbitals is weakened. The pCOHP of N–N bonds changes remarkably, and the −ICOHP value (12.9) of the N–N bonds is reduced by half compared with its value (26.4) in the absence of Ce atoms [Fig. 4(e)]. At this time, the N–N bond strength is close to that in $P2_1$–LiN_5 (−ICOHP = 15.3) at 32 GPa,[74] indicating that N≡N triple bonds have become N=N double or N–N single bonds. The reaction mechanism is similar to that in which Ce atoms are able to catalyze the production of NH_3 from N_2 through the breaking of N≡N triple bonds.[2] Although the Ce–N bonds exhibit an ionic bond interaction (−ICOHP = 2.1), the interaction between Ce_4*f* and N_2*p* orbitals plays a crucial role in the reaction [Figs. 4(e) and 4(f)]. Besides, each Ce atom provides 2.10*e* to N_2 molecules to assist their transformation to a polymerized N chain. More interestingly, the reaction Ce + $3N_2$ → *trans*-CeN_6 is exothermic, with an energy release of 3.19 eV/f.u. at 32 GPa, indicating that the above process tends to occur spontaneously under high pressure.

Laser heating is an effective method to produce metal polynitrides under high pressure. As shown in Fig. 4(g), $P\bar{1}$-CeN_6 should be obtainable from *trans*-CeN_6 by laser heating. Because the reaction *trans*-CeN_6 → $P\bar{1}$-CeN_6 is exothermic, with an energy release of 2.48 eV/f.u., the high-temperature environment could increase the anharmonic vibration of atoms and accelerate the conversion of thermodynamically unstable *trans*-CeN_6 into the stable phase $P\bar{1}$-CeN_6 at 32 GPa [Fig. S1(e) supplementary material]. Although the average −ICOHP of N–N bonds in $P\bar{1}$-CeN_6 (11.2) is a bit smaller than that in *trans*-CeN_6 (12.9) [Fig. 4(h)], the total number of N–N bonds increases from six to seven in a unit cell, and the total −ICOHP increases from 77.2 to 78.50. The larger −ICOHP (2.7) of Ce–N bonds and the greater amount of charge transferred (2.20*e*) for the Ce atom in $P\overline{1}$-CeN_6 mean that the Ce–N interaction becomes stronger than that in *trans*-CeN_6. As shown in Fig. 4(i), the PDOS near the Fermi level is remarkably different from that of *trans*-CeN_6, indicating that a new atomic coordinated environment is formed in $P\overline{1}$-CeN_6, which exhibits a more stable configuration than that of *trans*-CeN_6. According to Fig. S6 (supplementary material), $P\overline{1}$-CeN_6 is an insulator with a bandgap of 3.25 eV. It is obvious that the bandgap increases with increasing pressure, which is similar to the behavior of AlN_4, AlN_5, and N_{10} cages.[11,51,75] The reason for this is that the strong coupling interaction of sp^2 or sp^3 orbitals in adjacent N atoms reduces the energy of the bonding state (valence band) and increases the energy of the antibonding state (conduction band), resulting in an increase in the gap.

C. Stability under ambient conditions

Quenching down the high-pressure phase to ambient conditions is of great significance for the practical application of HEDMs. Here, we further confirm the stability of $P\overline{1}$-CeN_6 under ambient conditions. The calculated phonon dispersion curve and elastic constants indicate that $P\overline{1}$-CeN_6 possess dynamical and mechanical stability at ambient pressure [Fig. 5(a) and Table SIV (supplementary material)]. An AIMD simulation was also performed. At 300 and 1000 K, the total energy of $P\overline{1}$-CeN_6 fluctuates about the equilibrium position and the nitrogen skeleton remains intact, indicating that this material possesses thermal stability under ambient conditions and 1000 K [Fig. S7 (supplementary material)]. In the radial distribution functions (RDFs), the first sharp peaks of each line demonstrate the nearest N–N, Ce–N, and Ce–Ce distances. The nearest N–N and Ce–N distances of $P\overline{1}$-CeN_6 are 1.44 and 2.59 Å at 0 GPa and 300 K, which are larger than those at 32 GPa and 300 K (1.41 and 2.47 Å, respectively) [Figs. 5(b) and S8 (supplementary material)]. The nearest N–N and Ce–N distances at 1000 K (1.43 and 2.58 Å) are comparable to those at 300 K. To sum up, $P\overline{1}$-CeN_6 can be quenched to ambient conditions if synthesized. In addition, *C*2/*m*-CeN_3, $P\overline{1}$-CeN_3, and $P\overline{1}$-CeN_4 are also dynamically, mechanically, and thermally stable under ambient conditions [Figs. S7 and S9 and Table SIV (supplementary material)], and they can maintain thermal stability up to 1000, 700, and 400 K, respectively.

Usually, high nitrogen content and stability under ambient conditions are mutually exclusive. According to the analysis above, the stability of $P\overline{1}$-CeN_6 in a high-pressure environment results from the high coordination number of Ce atoms and from charge

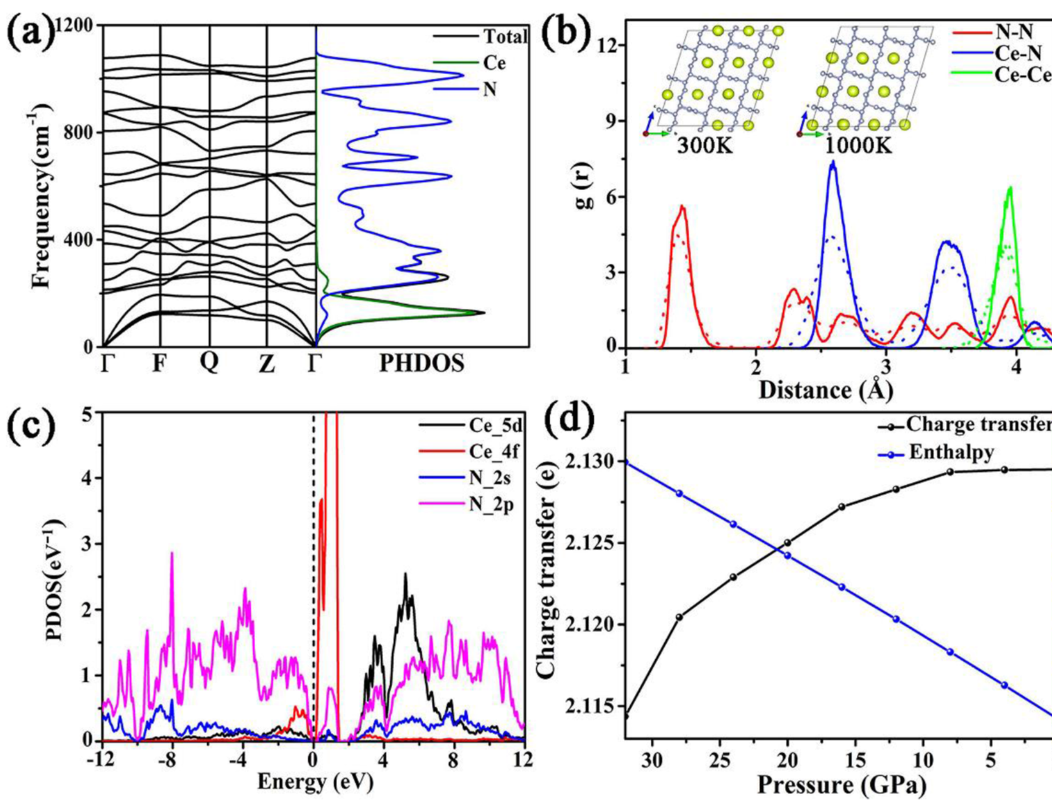

FIG. 5. (a) Phonon dispersion curve and PHDOS of $P\overline{1}$-CeN_6 at 0 GPa. (b) RDFs $g(r)$ and structures of final states from the last 2 ps of AIMD simulations at ambient pressure and temperatures of 300 K (solid lines) and 1000 K (dotted lines). (c) PDOS of $P\overline{1}$-CeN_6 at 0 GPa. (d) Curves of charge transfer and enthalpy as functions of pressure during pressure release in $P\overline{1}$-CeN_6, with the enthalpy of $P\overline{1}$-CeN_6 at 32 GPa being taken as the reference zero point.

TABLE I. Mass density ρ, mass energy density E_d, volumetric energy density E_v, detonation velocity V_d, and detonation pressure P_d of $P\bar{1}$-CeN_6 compared with those of TNT and HMX.

Compound	ρ (g/cm^3)	E_d (kJ/g)	E_v (kJ/cm^3)	V_d (km/s)	P_d (GPa)
$P\bar{1}$-CeN_6	5.60	2.00	11.20	13.60	128.95
TNT	1.64[a]	4.30[b]	7.05[c]	6.90[d]	19.00[a]
HMX	1.90[a]	5.70[b]	10.83[c]	9.10[d]	39.30[a]

[a] Reference 70.
[b] Reference 29.
[c] Reference 32.
[d] Reference 52.

transfer. Interestingly, as the pressure decreases to ambient, the PDOS shows that the DOS of N_2*p* orbitals in the valence band increases slightly and can hold more electrons [Fig. 5(c)]. The Bader charge analysis supports the same conclusions, with the amount of charge transferred increasing as the pressure decreases in $P\bar{1}$-CeN_6, indicating that the Ce atoms tend to provide more electrons at low pressure to enhance the stability of the N structure [Fig. 5(d)]. Meanwhile, the enthalpy decreases with decreasing pressure. Hence, charge transfer plays an important role in the stability of N structures at ambient pressure.

D. Energy density and explosive performance

The energy density, detonation velocity, and detonation pressure are important parameters to evaluate the explosive performance of an HEDM. Usually, these parameters are significantly related to the nitrogen content, the bonding types, and the mass of the coordination element. The mass energy density and volumetric energy density of $P\bar{1}$-CeN_6 are calculated using the dissociation path under ambient pressure: $P\bar{1}\text{-}CeN_6 \rightarrow CeN + \frac{5}{2}N_2$. As shown in Table I, the mass energy density of $P\bar{1}$-CeN_6 is 2.00 kJ/g, which is comparable to that of the reported CNO (2.2 kJ/g)[76] and LiN_5 (2.72 kJ/g),[74] and larger than that of *C*2/*m*-FeN_6 (1.83 kJ/g),[38] $P\bar{1}$-GdN_6 (1.62 kJ/g),[52] and *Ibam*-BaN_{10} (1.33 kJ/g).[30] Additionally, the volumetric energy density of $P\bar{1}$-CeN_6 is as high as 11.20 kJ/cm^3, which is larger than those of the high explosives TNT (7.05 kJ/cm^3) and HMX (10.83 kJ/cm^3) and those of some metal polynitrides (β-BeN_4, γ-BeN_4, GdN_6, ReN_8, BeN_{10}, MgN_{10}, BaN_{10}, CaN_{10}, YN_{10}, GaN_{15}, ScN_{15}, and YN_{15}) (3.46–10.95 kJ/cm^3), and close to the reported maximum value in Be–N compounds (12.7 kJ/cm^3).[29–32,39,40]

Interestingly, $P\bar{1}$-CeN_6 possesses outstanding detonation velocity V_d and detonation pressure P_d. Its detonation pressure is 128.95 GPa, which is about seven times that of TNT (19.00 GPa) and more than three times that of HMX (39.30 GPa), and its detonation velocity is 13.60 km/s, which is twice that of TNT (13.60 km/s). Moreover, the detonation pressure and velocity of $P\bar{1}$-CeN_6 are also greater than those of typical metal polynitrides, such as BeN_4, ScN_6, ScN_7, GdN_6, SnN_{20}, and MN_{10} (M = Be, Mg, Ba, Ca, and Y) and MN_{15} (M = Al, Ga, Sc, and Y) compounds (15.81–100.96 GPa and 5.22–13.04 km/s).[29–33,39,41] Notably, the excellent volumetric energy density, detonation pressure, and detonation velocity of $P\bar{1}$-CeN_6 are caused by its high mass density (up to 5.6 g/cm^3). Thus, $P\bar{1}$-CeN_6 exhibits excellent explosive properties as a novel HEDM under ambient pressure.

E. Mechanical properties

Mechanical properties are important for the practical application of Ce polynitrides. Hence, the bulk modulus *B*, shear modulus *G*, Young's modulus *E*, Poisson's ratio v, and Vickers hardness H_v of $P\bar{1}$-CeN_6 were calculated at ambient pressure (Table II). The C_{33} (469 GPa) of $P\bar{1}$-CeN_6 is greater than its C_{11} (273 GPa) and C_{22} (371 GPa), indicating greater incompressibility along the [001] directions than the [100] and [010] directions. The hardness of $P\bar{1}$-CeN_6 is 20.7 GPa, which is greater than those of AlN_5 (15.2 GPa), MnN_4 (17.5 GPa), HfN_{10} (13.7 GPa), NbN_4 (17.9 GPa), ScN_5 (17.4 GPa), ScN_3 (17.5 GPa), M-ReN_8, (13.9 GPa) and T′-ReN_8 (14.1 GPa), and comparable to those of FeN_6 (24.9 GPa), RuN_3 (23.4 GPa), and IrN_4 (22.4 GPa),[77–79] indicating that $P\bar{1}$-CeN_6 is a typical hard material (>20 GPa). The calculated Poisson's ratio of $P\bar{1}$-CeN_6 is 0.2. This low Poisson's ratio is the result of directional bonds, which increase the shear modulus and limit the movement of dislocations, increasing the hardness of the material.[77] The small *B*/*G* ratio (<1.75) reveals that $P\bar{1}$-CeN_6 is a brittle material.

Additionally, the material stiffness of $P\bar{1}$-CeN_6 is anisotropic. The 3D surface of the Young's modulus of $P\bar{1}$-CeN_6 is deformed [Fig. 6(a)], and the Young's modulus of $P\bar{1}$-CeN_6 along the *c* axis is higher than that along the other direction owing to the strong N–N covalent bonds, indicating that the layered structure with novel N_{14} rings along the [001] direction is more incompressible [Fig. 6(b)]. The degree of crystal anisotropy can be described quantitatively by the ratio E_{max}/E_{min}. The E_{max}/E_{min} value of $P\bar{1}$-CeN_6 is 2.40, which is less than those of *tr*-FeN_4 (3.74) and ReN_8 (4.95–13.49),[40] indicating a weaker crystal anisotropy.

F. IR and Raman spectra

The IR and Raman spectra of $P\bar{1}$-CeN_6 were calculated for experimental reference. From a group-theoretical analysis, the irreducible representation of $P\bar{1}$-CeN_6 is $\Gamma = 12A_u^I + 9A_g^R$. Therefore, $P\bar{1}$-CeN_6 has 18 vibrational modes after the removal of three acoustic modes ($3A_u^I$). In Fig. S10 (supplementary material),

TABLE II. Bulk modulus *B*, shear modulus *G*, Young's modulus *E*, Poisson's ratio v, and Vickers hardness H_v of $P\bar{1}$-CeN_6.

B (GPa)	*G* (GPa)	*E* (GPa)	v	H_v (GPa)	*B*/*G*
155.00	118.12	282.59	0.20	20.73	1.31

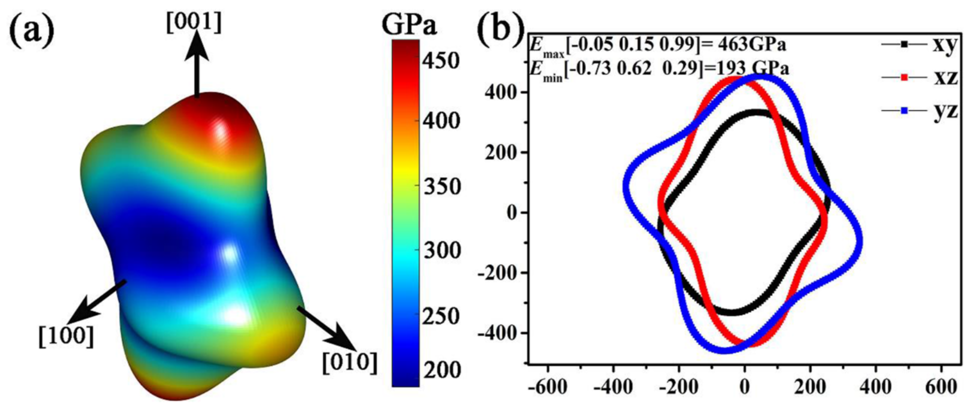

FIG. 6. (a) 3D surface and (b) 2D projected profiles of Young's modulus in $P\bar{1}$-CeN_6.

the modes of IR and Raman activity are denoted by I and R, respectively. The corresponding vibrational modes are presented in Figs. S11–S14 (supplementary material). $P\bar{1}$-CeN_6 contains 9 IR-active modes ($9A_u$) and 9 Raman-active modes ($9A_g$). At 32 GPa, both the A_u modes (274, 308, 355, 389, 509, 671, 683, 1009, and 1107 cm^{-1}) and A_g modes (465, 550, 674, 811, 947, 1011, 1036, 1078, and 1169 cm^{-1}) correspond to the out-of-plane N–N bending vibrations of folded N_{14} rings. At 0 GPa, both the A_u modes (169, 215, 220, 278, 439, 605, 625, 859, and 1003 cm^{-1}) and A_g modes (322, 481, 571, 699, 820, 875, 934, 967, and 1059 cm^{-1}) also correspond to out-of-plane N–N bending vibration in the layered N-structure.

IV. CONCLUSION

A systematic high-pressure study of CeN_n (n = 0.5, 1, 2, 3, 4, 5, and 6) compounds has been performed using first-principles swarm-intelligence structural searches. The phase diagram of CeN_n compounds has been enriched by the proposal of six new stable high-pressure phases ($I4/mmm$-CeN_2, $C2/m$-CeN_3, $P\bar{1}$-CeN_3, $P\bar{1}$-CeN_4, $C2/c$-CeN_6, and $P\bar{1}$-CeN_6). The stability of the new phases has been verified using the phonon dispersion curve, elastic constants, and AIMD simulations. The proposed layered structure of $P\bar{1}$-CeN_6 is composed of novel N_{14} ring. Not only does $P\bar{1}$-CeN_6 possess the lowest synthesis pressure of 32 GPa among the layered metal nitrides, but also it can be quenched down to ambient conditions. The reaction path Ce + $3N_2$ → *trans*-CeN_6 → $P\bar{1}$-CeN_6 has been proposed to clarify the formation mechanism of $P\bar{1}$-CeN_6 under high pressure. The calculated results for COHP and electronic structure reveal that the charge transfer and orbital hybridization of Ce and N atoms play a crucial role in stabilizing $P\bar{1}$-CeN_6. The volumetric energy density of $P\bar{1}$-CeN_6 reaches 11.20 kJ/cm^3, which is much higher than those of TNT and HMX. The detonation pressure (128.95 GPa) and detonation velocity (13.60 km/s) of $P\bar{1}$-CeN_6 are respectively almost seven times and twice those of TNT. Hence, $P\bar{1}$-CeN_6 has great application potential as an explosive material owing to its high stability and excellent explosive properties under ambient conditions.

SUPPLEMENTARY MATERIAL

See the supplementary material for supplementary figures and tables.

ACKNOWLEDGMENTS

This work was supported financially by the National Key R&D Program of China (Grant Nos. 2018YFA0305900 and 2018YFA0703404), the National Natural Science Foundation of China under Grant Nos. 21905159, 11634004, 51320105007, 11604116, and 51602124, the Program for Changjiang Scholars and Innovative Research Team in the University of the Ministry of Education of China under Grant No. IRT1132, the Higher Educational Youth Innovation Science and Technology Program Shandong Province (Grant No. 2022KJ183), and GHfund B (Grant No. 202202026143).

AUTHOR DECLARATIONS

Conflict of Interest

The authors have no conflicts to disclose.

Author Contributions

Yuanyuan Wang: Writing – original draft (equal). **Zhihui Li**: Investigation (equal). **Shifeng Niu**: Investigation (equal). **Wencai Yi**: Writing – review & editing (equal). **Shuang Liu**: Data curation (equal). **Zhen Yao**: Writing – review & editing (equal). **Bingbing Liu**: Writing – review & editing (equal).

DATA AVAILABILITY

The data supporting the findings of this study are available within the article and its supplementary material.

REFERENCES

[1] X. Q. Chen, C. L. Fu, and R. Podloucky, "Bonding and strength of solid nitrogen in the cubic gauche (cg-N) structure," Phys. Rev. B **77**, 064103 (2008).

[2] M. Sun, Y. Yin, and Z. Pang, "Predicted new structures of polymeric nitrogen under 100–600 GPa," Comput. Mater. Sci. **98**, 399–404 (2015).

[3] X. Wang, F. Tian, L. Wang, X. Jin, D. Duan, X. Huang, B. Liu, and T. Cui, "Predicted novel metallic metastable phases of polymeric nitrogen at high pressures," New J. Phys. **15**, 013010 (2013).

[4] X. Wang, F. Tian, L. Wang, T. Cui, B. Liu, and G. Zou, "Structural stability of polymeric nitrogen: A first-principles investigation," J. Chem. Phys. **132**, 024502 (2010).

[5]S. V. Bondarchuk and B. F. Minaev, "Two-dimensional honeycomb (A7) and zigzag sheet (ZS) type nitrogen monolayers. A first principles study of structural, electronic, spectral, and mechanical properties," Comput. Mater. Sci. **133**, 122–129 (2017).
[6]F. Zahariev, A. Hu, J. Hooper, F. Zhang, and T. Woo, "Layered single-bonded nonmolecular phase of nitrogen from first-principles simulation," Phys. Rev. B **72**, 214108 (2005).
[7]Y. Ma, A. R. Oganov, Z. Li, Y. Xie, and J. Kotakoski, "Novel high pressure structures of polymeric nitrogen," Phys. Rev. Lett. **102**, 065501 (2009).
[8]X. L. Wang, Z. He, Y. M. Ma, T. Cui, Z. M. Liu, B. B. Liu, J. F. Li, and G. T. Zou, "Prediction of a new layered phase of nitrogen from first-principles simulations," J. Phys.: Condens. Matter **19**, 425226 (2007).
[9]J. Kotakoski and K. Albe, "First-principles calculations on solid nitrogen: A comparative study of high-pressure phases," Phys. Rev. B **77**, 144109 (2008).
[10]W. D. Mattson, D. Sanchez-Portal, S. Chiesa, and R. M. Martin, "Prediction of new phases of nitrogen at high pressure from first-principles simulations," Phys. Rev. Lett. **93**, 125501 (2004).
[11]X. Wang, Y. Wang, M. Miao, X. Zhong, J. Lv, T. Cui, J. Li, L. Chen, C. J. Pickard, and Y. Ma, "Cagelike diamondoid nitrogen at high pressures," Phys. Rev. Lett. **109**, 175502 (2012).
[12]M. I. Eremets, A. G. Gavriliuk, I. A. Trojan, D. A. Dzivenko, and R. Boehler, "Single-bonded cubic form of nitrogen," Nat. Mater. **3**, 558–563 (2004).
[13]D. Tomasino, M. Kim, J. Smith, and C. S. Yoo, "Pressure-induced symmetry-lowering transition in dense nitrogen to layered polymeric nitrogen (LP-N) with colossal Raman intensity," Phys. Rev. Lett. **113**, 205502 (2014).
[14]D. Laniel, G. Geneste, G. Weck, M. Mezouar, and P. Loubeyre, "Hexagonal layered polymeric nitrogen phase synthesized near 250 GPa," Phys. Rev. Lett. **122**, 066001 (2019).
[15]D. Laniel, B. Winkler, T. Fedotenko, A. Pakhomova, S. Chariton, V. Milman, V. Prakapenka, L. Dubrovinsky, and N. Dubrovinskaia, "High-pressure polymeric nitrogen allotrope with the black phosphorus structure," Phys. Rev. Lett. **124**, 216001 (2020).
[16]D. Laniel, G. Weck, G. Gaiffe, G. Garbarino, and P. Loubeyre, "High-pressure synthesized lithium pentazolate compound metastable under ambient conditions," J. Phys. Chem. Lett. **9**, 1600–1604 (2018).
[17]Y. Wang, M. Bykov, I. Chepkasov, A. Samtsevich, E. Bykova, X. Zhang, S. Q. Jiang, E. Greenberg, S. Chariton, V. B. Prakapenka, A. R. Oganov, and A. F. Goncharov, "Stabilization of hexazine rings in potassium polynitride at high pressure," Nat. Chem. **14**, 794–800 (2022).
[18]D. Laniel, B. Winkler, E. Koemets, T. Fedotenko, M. Bykov, E. Bykova, L. Dubrovinsky, and N. Dubrovinskaia, "Synthesis of magnesium-nitrogen salts of polynitrogen anions," Nat. Commun. **10**, 4515 (2019).
[19]B. A. Steele, E. Stavrou, J. C. Crowhurst, J. M. Zaug, V. B. Prakapenka, and I. I. Oleynik, "High-pressure synthesis of a pentazolate salt," Chem. Mater. **29**, 735–741 (2016).
[20]D. Laniel, A. A. Aslandukova, A. N. Aslandukov, T. Fedotenko, S. Chariton, K. Glazyrin, V. B. Prakapenka, L. S. Dubrovinsky, and N. Dubrovinskaia, "High-pressure synthesis of the beta-Zn_3N_2 nitride and the alpha-ZnN_4 and beta-ZnN_4 polynitrogen compounds," Inorg. Chem. **60**, 14594–14601 (2021).
[21]M. Bykov, T. Fedotenko, S. Chariton, D. Laniel, K. Glazyrin, M. Hanfland, J. S. Smith, V. B. Prakapenka, M. F. Mahmood, A. F. Goncharov, A. V. Ponomareva, F. Tasnadi, A. I. Abrikosov, T. Bin Masood, I. Hotz, A. N. Rudenko, M. I. Katsnelson, N. Dubrovinskaia, L. Dubrovinsky, and I. A. Abrikosov, "High-pressure synthesis of Dirac materials: Layered van der Waals bonded BeN_4 polymorph," Phys. Rev. Lett. **126**, 175501 (2021).
[22]M. Zhang, H. Yan, and Q. Wei, "Une xpected ground-state crystal structures and mechanical properties of transition metal pernitrides MN_2 (M = Ti, Zr, and Hf)," J. Alloys Compd. **774**, 918–925 (2019).
[23]J. Zhang, X. Li, X. Dong, H. Dong, A. R. Oganov, and J. M. McMahon, "Theoretical study of the crystal structure, stability, and properties of phases in the V-N system," Phys. Rev. B **104**, 134111 (2021).
[24]X. Wang, J. Li, J. Botana, M. Zhang, H. Zhu, L. Chen, L. Liu, T. Cui, and M. Miao, "Polymerization of nitrogen in lithium azide," J. Chem. Phys. **139**, 164710 (2013).
[25]X. Wang, J. Li, H. Zhu, L. Chen, and H. Lin, "Polymerization of nitrogen in cesium azide under modest pressure," J. Chem. Phys. **141**, 044717 (2014).
[26]M. Zhang, K. Yin, X. Zhang, H. Wang, Q. Li, and Z. Wu, "Structural and electronic properties of sodium azide at high pressure: A first principles study," Solid State Commun. **161**, 13–18 (2013).
[27]J. Lin, F. Wang, Q. Rui, J. Li, Q. Wang, and X. Wang, "A novel square planar N_4^{2-} ring with aromaticity in BeN_4," Matter Radiat. Extremes **7**, 038401 (2022).
[28]S. Niu, D. Xu, H. Li, Z. Yao, S. Liu, C. Zhai, K. Hu, X. Shi, P. Wang, and B. Liu, "Pressure-stabilized polymerization of nitrogen in manganese nitrides at ambient and high pressures," Phys. Chem. Chem. Phys. **24**, 5738 (2022).
[29]K. Xia, X. Zheng, J. Yuan, C. Liu, H. Gao, Q. Wu, and J. Sun, "Pressure-stabilized high-energy-density alkaline-earth-metal pentazolate salts," J. Phys. Chem. C **123**, 10205–10211 (2019).
[30]J. Yuan, K. Xia, J. Wu, and J. Sun, "High-energy-density pentazolate salts: CaN_{10} and BaN_{10}," Sci. China-Phys. Mech. Astron. **64**, 218211 (2020).
[31]W. Lu, K. Hao, S. Liu, J. Lv, M. Zhou, and P. Gao, "Pressure-stabilized high-energy-density material YN_{10}," J. Phys.: Condens. Matter **34**, 135403 (2022).
[32]K. Xia, J. Yuan, X. Zheng, C. Liu, H. Gao, Q. Wu, and J. Sun, "Predictions on high-power trivalent metal pentazolate salts," J. Phys. Chem. Lett. **10**, 6166–6173 (2019).
[33]B. Wang, R. Larhlimi, H. Valencia, F. Guégan, and G. Frapper, "Prediction of novel tin nitride Sn_xN_y phases under pressure," J. Phys. Chem. C **124**, 8080–8093 (2020).
[34]W. Yi, L. Zhao, X. Liu, X. Chen, Y. Zheng, and M. Miao, "Packing high-energy together: Binding the power of pentazolate and high-valence metals with strong bonds," Mater. Des. **193**, 108820 (2020).
[35]J. Zhang, Z. Zeng, H. Q. Lin, and Y. L. Li, "Pressure-induced planar N_6 rings in potassium azide," Sci. Rep. **4**, 4358 (2014).
[36]K. Xia, H. Gao, C. Liu, J. Yuan, J. Sun, H. T. Wang, and D. Xing, "A novel superhard tungsten nitride predicted by machine-learning accelerated crystal structure search," Sci. Bull. **63**, 817–824 (2018).
[37]Z. Liu, D. Li, Q. Zhuang, F. Tian, D. Duan, F. Li, and T. Cui, "Formation mechanism of insensitive tellurium hexanitride with armchair-like cyclo-N_6 anions," Commun. Chem. **3**, 42 (2020).
[38]L. Wu, R. Tian, B. Wan, H. Liu, N. Gong, P. Chen, T. Shen, Y. Yao, H. Gou, and F. Gao, "Prediction of stable iron nitrides at ambient and high pressures with progressive formation of new polynitrogen species," Chem. Mater. **30**, 8476–8485 (2018).
[39]X. Zhang, X. Xie, H. Dong, X. Zhang, F. Wu, Z. Mu, and M. Wen, "Pressure-induced high-energy-density BeN_4 materials with nitrogen chains: First-principles study," J. Phys. Chem. C **125**, 25376–25382 (2021).
[40]L. Wu, P. Zhou, Y. Li, B. Wan, S. Sun, J. Xu, J. Sun, B. Liao, and H. Gou, "Ultra-incompressibility and high energy density of ReN_8 with infinite nitrogen chains," J. Mater. Sci. **56**, 3814–3826 (2020).
[41]Y. Guo, S. Wei, Z. Liu, H. Sun, G. Yin, S. Chen, Z. Yu, Q. Chang, and Y. Sun, "Polymerization of nitrogen in two theoretically predicted high-energy compounds ScN_6 and ScN_7 under modest pressure," New J. Phys. **24**, 083015 (2022).
[42]J. Zhang, A. R. Oganov, X. Li, and H. Niu, "Pressure-stabilized hafnium nitrides and their properties," Phys. Rev. B **95**, 020103 (2017).
[43]S. Yu, B. Huang, Q. Zeng, A. R. Oganov, L. Zhang, and G. Frapper, "Emergence of novel polynitrogen molecule-like species, covalent chains, and layers in magnesium–nitrogen Mg_xN_y phases under high pressure," J. Phys. Chem. C **121**, 11037–11046 (2017).
[44]B. Huang and G. Frapper, "Barium–nitrogen phases under pressure: Emergence of structural diversity and nitrogen-rich compounds," Chem. Mater. **30**, 7623–7636 (2018).
[45]J. Lin, D. Peng, Q. Wang, J. Li, H. Zhu, and X. Wang, "Stable nitrogen-rich scandium nitrides and their bonding features under ambient conditions," Phys. Chem. Chem. Phys. **23**, 6863–6870 (2021).
[46]S. Liu, R. Liu, H. Li, Z. Yao, X. Shi, P. Wang, and B. Liu, "Cobalt-nitrogen compounds at high pressure," Inorg. Chem. **60**, 14022–14030 (2021).
[47]S. Niu, Z. Li, H. Li, X. Shi, Z. Yao, and B. Liu, "New cadmium-nitrogen compounds at high pressures," Inorg. Chem. **60**, 6772–6781 (2021).
[48]B. A. Steele and I. I. Oleynik, "Novel potassium polynitrides at high pressures," J. Phys. Chem. A **121**, 8955–8961 (2017).

[49]S. Wei, D. Li, Z. Liu, W. Wang, F. Tian, K. Bao, D. Duan, B. Liu, and T. Cui, "A novel polymerization of nitrogen in beryllium tetranitride at high pressure," J. Phys. Chem. C **121**, 9766–9772 (2017).
[50]J. Hou, X. J. Weng, A. R. Oganov, X. Shao, G. Gao, X. Dong, H. T. Wang, Y. Tian, and X. F. Zhou, "Helium-nitrogen mixtures at high pressure," Phys. Rev. B **103**, L060102 (2021).
[51]Z. Liu, D. Li, Y. Liu, T. Cui, F. Tian, and D. Duan, "Metallic and anti-metallic properties of strongly covalently bonded energetic AlN_5 nitrides," Phys. Chem. Chem. Phys. **21**, 12029 (2019).
[52]L. Liu, D. Wang, S. Zhang, and H. Zhang, "Pressure-stabilized GdN_6 with an armchair–antiarmchair structure as a high energy density material," J. Mater. Chem. A **9**, 16751–16758 (2021).
[53]H. Cai, X. Wang, Y. Zheng, X. Jiang, J. Zeng, Y. Feng, and K. Chen, "Prediction of erbium–nitrogen compounds as high-performance high-energy-density materials," J. Phys.: Condens. Matter **35**, 085701 (2023).
[54]X. Hu, Y. Sun, S. Guo, J. Sun, Y. Fu, S. Chen, S. Zhang, and J. Zhu, "Identifying electrocatalytic activity and mechanism of $Ce_{1/3}NbO_3$ perovskite for nitrogen reduction to ammonia at ambient conditions," Appl. Catal., B **280**, 119419 (2021).
[55]J. Qi, S. Zhou, K. Xie, and S. Lin, "Catalytic role of assembled Ce Lewis acid sites over ceria for electrocatalytic conversion of dinitrogen to ammonia," J. Energy Chem. **60**, 249–258 (2021).
[56]B. Xu, L. Xia, F. Zhou, R. Zhao, H. Chen, T. Wang, Q. Zhou, Q. Liu, G. Cui, X. Xiong, F. Gong, and X. Sun, "Enhancing electrocatalytic N_2 reduction to NH_3 by CeO_2 nanorod with oxygen vacancies," ACS Sustainable Chem. Eng. **7**, 2889–2893 (2019).
[57]V. Kanchana, G. Vaitheeswaran, X. Zhang, Y. Ma, A. Svane, and O. Eriksson, "Lattice dynamics and elastic properties of the 4*f* electron system: CeN," Phys. Rev. B **84**, 205135 (2011).
[58]M. B. Nielsen, D. Ceresoli, J.-E. Jørgensen, C. Prescher, V. B. Prakapenka, and M. Bremholm, "Experimental evidence for pressure-induced first order transition in cerium nitride from B1 to B10 structure type," J. Appl. Phys. **121**, 025903 (2017).
[59]M. Zhang, H. Yan, Q. Wei, and H. Wang, "Exploration on pressure-induced phase transition of cerium mononitride from first-principles calculations," Appl. Phys. Lett. **102**, 231901 (2013).
[60]Y. Wang, J. Lv, L. Zhu, and Y. Ma, "CALYPSO: A method for crystal structure prediction," Comput. Phys. Commun. **183**, 2063–2070 (2012).
[61]J. F. l. G. Kresse, "Efficient iterative schemes for a*b initio* total-energy calculations using a plane-wave basis set," Phys. Rev. B **54**, 11169–11186 (1996).
[62]K. Burke, J. P. Perdew, and M. Ernzerhof, "Generalized gradient approximation made simple," Phys. Rev. Lett. **77**, 3865–3868 (1996).
[63]A. M. Hao and J. Bai, "First-principles calculations of electronic and magnetic properties of CeN: The LDA + *U* method," Chin. Phys. B **22**, 107102 (2013).
[64]Y. G. Zhang, G. B. Zhang, and Y. X. Wang, "First-principles study of the electronic structure and optical properties of Ce-doped ZnO," J. Appl. Phys. **109**, 063510 (2011).
[65]T. Zacherle, A. Schriever, R. A. De Souza, and M. Martin, "*Ab initio* analysis of the defect structure of ceria," Phys. Rev. B **87**, 134104 (2013).
[66]C. W. M. Castleton, J. Kullgren, and K. Hermansson, "Tuning for electron localization and structure at oxygen vacancies in ceria," J. Chem. Phys. **127**, 244704 (2007).
[67]D. J. G. Kresse, "From ultrasoft pseudopotentials to the projector augmented-wave method," Phys. Rev. B **59**, 1758–1775 (1999).
[68]A. V. Krukau, G. E. Scuseria, J. P. Perdew, and A. Savin, "Hybrid functionals with local range separation," J. Chem. Phys. **129**, 124103 (2008).
[69]A. Togo, L. Chaput, and I. Tanaka, "Distributions of phonon lifetimes in Brillouin zones," Phys. Rev. B **91**, 094306 (2015).
[70]M. J. K. a. C. Dickinson, "Evaluation of the simplied calculational method for Chapman-Jouguet detonation pressures on the basis of available experimental information," J. Chem. Phys. **48**, 43–50 (1968).
[71]M. Parrinello and A. Rahman, "Crystal structure and pair potentials: A molecular-dynamics study," Phys. Rev. Lett. **45**, 1196–1199 (1980).
[72]V. L. Deringer, A. L. Tchougreeff, and R. Dronskowski, "Crystal orbital Hamilton population (COHP) analysis as projected from plane-wave basis sets," J. Phys. Chem. A **115**, 5461–5466 (2011).
[73]M. D. Segall, P. J. D. Lindan, M. J. Probert, C. J. Pickard, P. J. Hasnip, S. J. Clark, and M. C. Payne, "First-principles simulation: Ideas, illustrations and the CASTEP code," J. Phys.: Condens. Matter **14**, 2717–2744 (2002).
[74]F. Peng, Y. Yao, H. Liu, and Y. Ma, "Crystalline LiN_5 predicted from first-principles as a possible high-energy material," J. Phys. Chem. Lett. **6**, 2363–2366 (2015).
[75]S. Ma, F. Peng, S. Zhu, S. Li, and T. Gao, "Novel phase of AlN_4 as a possible superhard material," J. Phys. Chem. C **122**, 22660–22666 (2018).
[76]Z. Raza, C. J. Pickard, C. Pinilla, and A. M. Saitta, "High energy density mixed polymeric phase from carbon monoxide and nitrogen," Phys. Rev. Lett. **111**, 235501 (2013).
[77]Z. Zhao, K. Bao, F. Tian, D. Duan, B. Liu, and T. Cui, "Phase diagram, mechanical properties, and electronic structure of Nb-N compounds under pressure," Phys. Chem. Chem. Phys. **17**, 22837–22845 (2015).
[78]Y. Zhang, L. Wu, B. Wan, Y. Lin, Q. Hu, Y. Zhao, R. Gao, Z. Li, J. Zhang, and H. Gou, "Diverse ruthenium nitrides stabilized under pressure: A theoretical prediction," Sci. Rep. **6**, 33506 (2016).
[79]X. Du, Y. Yao, J. Wang, Q. Yang, and G. Yang, "IrN_4 and IrN_7 as potential high-energy-density materials," J. Chem. Phys. **154**, 054706 (2021).